Pulmonary Ventilation Imaging Based on 4-Dimensional Computed Tomography: Comparison With Pulmonary Function Tests and SPECT Ventilation Images

Tokihiro Yamamoto PhD[*†], Sven Kabus PhD[‡], Cristian Lorenz PhD[‡], Erik Mittra MD, PhD[§], Julian C. Hong MS[*], Melody Chung BS[*], Neville Eclov BS[*], Jacqueline To BS[*], Maximilian Diehn MD, PhD[*], Billy W. Loo Jr.MD, PhD[*], Paul J. Keall PhD[‖]

[*] Department of Radiation Oncology, Stanford University School of Medicine, Stanford, California

[†] Department of Radiation Oncology, University of California Davis School of Medicine, Sacramento, California

[‡] Department of Digital Imaging, Philips Research Europe, Hamburg, Germany

[§] Departments of Radiology, Stanford University School of Medicine, Stanford, California

[‖] Radiation Physics Laboratory, Sydney Medical School, University of Sydney, Sydney, New South Wales, Australia

Corresponding Author: Tokihiro Yamamoto PhD. Department of Radiation Oncology, University of California Davis School of Medicine, 4501 X St, Sacramento, CA 95817. Tel: (916) 734-0604; E-mail: toyamamoto@ ucdavis.edu

This study was supported in part by a National Lung Cancer Partnership Young Investigator Research grant and National Institutes of Health/ National Cancer Institute grant R01 CA 093626. Conflict of interest: Dr Yamamoto receives nonfinancial support from Philips Radiation Oncology Systems. Drs Kabus and Lorenz are employees of Philips Research. Dr Keall holds a patent for a method and system for using computed tomography to test pulmonary function (U.S. 7668357 issued).

Acknowledgments: Michael Goris, MD, PhD, and Lindee Burton, Department of Radiology, Stanford, provided support for the clinical trial. Eric Johnston, Department of Electrical Engineering, Stanford, assisted with 4D-CT sorting. Lihong Qi, PhD, Department of Public Health Sciences, University of California Davis, provided advice on estimating the statistical power of the analysis. Philips Radiation, Oncology Systems, lent us Pinnacle3 treatment planning systems.

Summary

We compared 4-dimensional computed tomography (4DCT) ventilation imaging, an emerging functional imaging modality, with pulmonary function test measurements and single-photon emission CT (SPECT) ventilation images, which are the clinical references for global and regional lung function, respectively. An 18-patient study demonstrated significant correlations between 4D-CT ventilation images and pulmonary function test as well as single-photon emission CT ventilation images, providing evidence toward validation of 4D-CT ventilation imaging.

Purpose

4-dimensional computed tomography (4D-CT)-based pulmonary ventilation imaging is an emerging functional imaging modality. The purpose of this study was to investigate the physiological significance of 4D-CT ventilation imaging by comparison with pulmonary function test (PFT) measurements and single-photon emission CT (SPECT) ventilation images, which are the clinical references for global and regional lung function, respectively.

Methods and Materials

In an institutional review board–approved prospective clinical trial, 4D-CT imaging and PFT and/or SPECT ventilation imaging were performed in thoracic cancer patients. Regional ventilation (V_{4DCT}) was calculated by deformable image registration of 4D-CT images and quantitative analysis for regional volume change. V_{4DCT} defect parameters were compared with the PFT measurements (forced expiratory volume in 1 second (FEV_1; % predicted) and FEV_1/forced vital capacity (FVC; %). V_{4DCT} was also compared with SPECT ventilation (V_{SPECT}) to *(1)* test whether V_{4DCT} in V_{SPECT} defect regions is significantly lower than in nondefect regions by using the 2-tailed *t* test; *(2)* to quantify the spatial overlap between V_{4DCT} and V_{SPECT} defect regions with Dice similarity coefficient (DSC); and *(3)* to test ventral-to-dorsal gradients by using the 2-tailed *t* test.

Results

Of 21 patients enrolled in the study, 18 patients for whom 4D-CT and either PFT or SPECT were acquired were included in the analysis. V_{4DCT} defect parameters were found to have significant, moderate correlations with PFT measurements. For example, V4DCTHU defect volume increased significantly with decreasing FEV_1/FVC ($R=-0.65$, $P<.01$). V_{4DCT} in V_{SPECT} defect regions was significantly lower than in nondefect regions (mean V4DCTHU 0.049 vs 0.076, $P<.01$). The average DSCs for the spatial overlap with SPECT ventilation defect regions were only moderate (V4DCTHU0.39 ± 0.11). Furthermore, ventral-to-dorsal gradients of V_{4DCT} were strong (V4DCTHU $R^2 = 0.69$, $P=.08$), which was similar to V_{SPECT} ($R^2 = 0.96$, $P<.01$).

Conclusions

An 18-patient study demonstrated significant correlations between 4D-CT ventilation and PFT measurements as well as SPECT ventilation, providing evidence toward the validation of 4D-CT ventilation imaging.

Introduction

Despite technological advances in the field, overall survival of lung cancer remains disappointing, and toxicity is substantial. Radiation pneumonitis is a common, potentially fatal toxicity that occurs in up to 30% of lung cancer patients treated with radiation therapy 1, 2, 3. Radiation therapy that selectively avoids irradiating highly functional lung regions may reduce pulmonary toxicity. This hypothesis is supported by several reports in the literature demonstrating that pulmonary toxicity correlates more strongly with the functional dose-volume parameters than the anatomic parameters (current clinical standard) 4, 5, 6. For example, Vinogradskiy et al (6) found that the functional (ventilation) parameters (eg, functional mean lung dose) had stronger correlations with grade ≥3 pneumonitis than the anatomic parameters (eg, mean lung dose) for 96 non-small cell lung cancer (NSCLC) patients (6).

There have been many modalities for pulmonary ventilation imaging, including single-photon emission computed tomography (SPECT) (7), positron emission tomography (PET) (8), magnetic resonance (MR) 9, 10, 11, and dual-energy CT (12). Ventilation images can also be acquired by an emerging technique based on 4-dimensional (4D) or biphasic (exhalation and inhalation) CT, deformable image registration (DIR) and quantitative analysis 13, 14, 15. Compared to other modalities, 4D-CT ventilation imaging has a higher resolution (the exact spatial resolution is unknown), lower cost, shorter scan time, and/or greater availability. 4D-CT ventilation can be considered "free" information for lung cancer patients treated with radiation therapy 14, 16, as 4D-CT scans are currently in routine use for radiation therapy at most centers (17) and ventilation computation involves only image processing and analysis. Prior to clinical applications, 4D-CT ventilation imaging should be validated against ground truth. Animal studies have demonstrated strong correlations between 4D-CT ventilation and xenon CT ventilation 15, 18, and also high reproducibility (19). However, human studies have reported inconsistent results 19, 20, 21, 22; for example, reasonable correlations have been found with hyperpolarized 3He MR ventilation (21), whereas weak correlations have been found with technetium-99m-labeled diethylenetriamine pentaacetate (99mTc-DTPA) SPECT ventilation images (20). Also, only poor-to-moderate reproducibility has been demonstrated 19, 22. These results suggest the need for further validation. The purpose of this study was to investigate the physiological significance of 4D-CT ventilation imaging by comparison with (1) pulmonary function test (PFT) measurements as the clinical reference for global lung function; and (2) ^{99m}Tc-DTPA SPECT ventilation images as the clinical reference for regional ventilation for patients with thoracic cancer.

Methods and Materials

Study design

This study was a prospective, single-arm, single-institutional clinical trial approved by the institutional review board. All patients provided written informed consent. Patients were eligible for participation if they had a primary or metastatic thoracic cancer to be treated with radiation therapy and were ≥18 years of age. We performed 4D-CT imaging (standard of care) as well as PFT and/or SPECT ventilation imaging with an attempt to acquire all the data prior to treatment (Supplementary Fig. S1).

4D-CT ventilation imaging

The first step of 4D-CT ventilation imaging was acquiring 4D-CT scans in the supine posture, using a Discovery ST multislice PET/CT scanner (GE Healthcare, Waukesha, WI). Scan parameters were 120 kVp, approximately 100 mAs per slice, 0.5-second gantry rotation, 0.45-second cine interval, and 2.5-mm slice thickness. CT data segments were then sorted into 10 respiratory bins by the phase-based method using Advantage 4D software (GE Healthcare) and anatomic similarity-based method designed to reduce artifacts (23). The resulting 4D-CT image with fewer 4D-CT artifacts was identified qualitatively and quantitatively by using the normalized cross correlation-based artifact score (24) and was selected for ventilation computation and subsequent analysis.

The second step was DIR for spatial mapping of the peak inhalation 4D-CT image (moving) to the peak exhalation image (fixed). We used a volumetric elastic DIR method that minimizes both a similarity function (sum of squared difference between the peak exhalation and deformed peak inhalation 4D-CT images) and a regularization term (elastic regularization) based on the Navier-Lamé equation. Further details of the algorithm have been described elsewhere (25). The registration accuracy was previously studied by quantifying the target registration error for anatomic landmarks in the lung, which were found to be less than the voxel dimension on average 25, 26, 27. The algorithm was evaluated in the MICCAI EMPIRE10 Challenge and placed 8th among 34 participants (27). Note that the accuracy for the cohort of patients used in this study has not been evaluated.

The final step was to quantify regional volume change per lung voxel volume, yielding a 4D-CT ventilation image at the peak exhalation phase (V_{4DCT}). We investigated 2 different metrics: Hounsfield unit (HU) change-based metric (V_{4DCT}^{HU}) and a Jacobian-based metric (V_{4DCT}^{Jac}). $V_{4DCT}^{HU}$was defined based on the relationship between the regional HU change and regional volume change 13, 28 as well as CT density scaling, expressed as

$$V_{4\mathrm{DCT}}^{\mathrm{HU}}(x,y,z)=\frac{\mathrm{HU}_{ex}(x,y,z)-\mathrm{HU}_{\mathrm{in}}\{x+u_x(x,y,z),y+u_y(x,y,z),z+u_z(x,y,z)\}}{\mathrm{HU}_{\mathrm{in}}\{x+u_x(x,y,z),y+u_y(x,y,z),z+u_z(x,y,z)\}+1000}\rho_{\mathrm{scaling}},$$

where HU is the HU value, *u* is the displacement vector mapping the voxel at location (*x*,*y*,*z*) of a peak exhalation image to the corresponding location of a peak inhalation image, and ρscaling is the CT density scaling factor ρscaling=(HU_{ex}+1024)/774, which takes a value ranging from 0 for the voxel with the lowest lung CT density (−1024 HU) to 1 for the voxel with the highest density (−250 HU), in a manner similar to that in Kipritidis et al (29). The rationale for density scaling is to transform a purely mechanical model of regional ventilation based on volume change alone to a more physiological model. Gas transport to high alveolar density regions contributes more to gas exchange and, hence, is considered more physiologically relevant than gas transport to low alveolar density regions. It was assumed that alveolar density was proportional to CT density. In the same manner as that described by Guerrero et al (14), mass correction was applied to HU_{in} to account for the differences in lung mass between the peak exhalation and peak inhalation phases. V_{4DCT}^{Jac} was defined by

$$V_{4\mathrm{DCT}}^{\mathrm{Jac}}(x,y,z)=\left\{\begin{vmatrix} 1+\frac{\partial u_x(x,y,z)}{\partial x} & \frac{\partial u_x(x,y,z)}{\partial y} & \frac{\partial u_x(x,y,z)}{\partial z} \\ \frac{\partial u_y(x,y,z)}{\partial x} & 1+\frac{\partial u_y(x,y,z)}{\partial y} & \frac{\partial u_y(x,y,z)}{\partial z} \\ \frac{\partial u_z(x,y,z)}{\partial x} & \frac{\partial u_z(x,y,z)}{\partial y} & 1+\frac{\partial u_z(x,y,z)}{\partial z} \end{vmatrix}-1\right\}\rho_{\mathrm{scaling}}.$$

The detailed derivation of the equations for V_{4DCT}^{HU} and V_{4DCT}^{Jac}, is described in the Appendix. For both V_{4DCT}^{HU} and V_{4DCT}^{Jac}, a value <0 indicated regional contraction, and a value >0 indicated regional expansion. The lung parenchyma was segmented by delineating lung voxels with less than (or equal to) −250 HU (14) within the lung outlines generated by the model-based segmentation of a Pinnacle³ radiation therapy treatment planning system (Philips Radiation Oncology Systems, Fitchburg, WI).

Comparison of 4D-CT ventilation defect parameters with PFT measurements

PFTs were performed to measure forced expiratory volume in 1 second (FEV_1 [% predicted]), forced vital capacity (FVC [% predicted]), FEV_1/FVC (%), and diffusing capacity of the lung for carbon monoxide (DL_{co} [% predicted]) with an HDpft system (nSpire Health, Longmont, CO) according to American Thoracic Society (ATS)/European Respiratory Society (ERS) guidelines (30). FEV_1 and FEV_1/FVC were chosen to analyze correlation with V_{4DCT} defect parameters, using the Pearson correlation, given that these parameters have been found to correlate significantly with hyperpolarized gas MR ventilation defect parameters 31, 32. We investigated the following V_{4DCT} defect parameters: (*1*) the lowest 25th percentile V_{4DCT} value; (*2*)

the absolute defect volume (l); and (*3*) the percentage defect volume. Given that no data are available on 4D-CT ventilation threshold values to identify defect regions, the threshold was determined by finding a value which gave the average percentage of defect volume of approximately 25%. Mathew et al 21, 33 found the average percentage defect volume of 25% for a similar cohort of patients by using hyperpolarized ^{3}He MR ventilation imaging. The threshold was found to be 0.015, yielding the mean volume of 1.1 ± 1.4 l (25% ± 21% of the total lung volume) for V_{4DCT}^{HU} and 1.2 ± 1.5 l (25 ± 20%) for V_{4DCT}^{Jac}.

Comparison of 4D-CT ventilation with SPECT ventilation images

V_{4DCT} was compared with V_{SPECT} to (*1*) test whether V_{4DCT} in V_{SPECT} defect regions was significantly lower than in nondefect regions; (*2*) quantify the spatial overlap between $V_{4DCT}$and V_{SPECT} defect regions; and (*3*) test ventral-to-dorsal gradients. V_{SPECT} scans and low-dose CT scans for attenuation correction were acquired in the supine posture with an Infinia Hawkeye (GE Healthcare) SPECT/CT scanner. ^{99m}Tc-DTPA was aerosolized using an Insta/Vent system (Medi/Nuclear, Baldwin Park, CA) and was then administered to the patient in the supine posture through slow, moderately deep breathing. SPECT projections were acquired in a 64 × 64 matrix with an 8.8- × 8.8-mm^2 pixel size, 8.8-mm slice spacing, 60 projections over 360°, and 30 seconds per projection during tidal breathing. SPECT images were reconstructed using the 3D ordered subsets expectation maximization (OSEM) algorithm (34) with attenuation correction. The low-dose CT image of SPECT was rigidly aligned with the peak exhalation 4D-CT image, using the Pinnacle^3 system. Central airways (plus a 1-cm margin) which were manually delineated using the Pinnacle^3 system, were excluded from all comparisons of V_{4DCT} and V_{SPECT}, considering central airway depositions of ^{99m}Tc-DTPA aerosols observed frequently in patients with chronic obstructive pulmonary disease (COPD) (7).

V_{SPECT} defect regions were segmented by delineating lung voxels with a value less than a threshold, which was determined as the mean intensity of the background noise plus twice the standard deviation of the distribution of the background noise in a manner similar to that used by Kauczor et al (35), yielding the mean volume of 24% ± 11% of the total lung volume. V_{4DCT} defect regions were segmented by the method described earlier. The 2-tailed *t* test was used to examine whether V_{4DCT} in V_{SPECT} defect regions is significantly lower than in nondefect regions (P<.05). The Dice similarity coefficient (DSC) (36) was used to quantify the spatial overlap between V_{4DCT} and V_{SPECT} defect regions. Furthermore, ventral-to-dorsal gradient was evaluated to determine whether 4D-CT ventilation imaging shows the known effect of gravity on ventilation (ie, greater ventilation in the dorsal region than in the ventral region due to the lung parenchyma tissue shift toward gravity-dependent region). This effect has been demonstrated with other imaging modalities 11, 37, 38. We quantified the slope (regression coefficient) from linear regression for the relationship between the relative ventral-to-dorsal distance and globally normalized ventilation value at the corresponding distance. The total lung was divided into 5 coronal section regions of interest, equally spaced along the ventral-to-dorsal direction. The mean ventilation value was quantified for each region of interest. Statistical analysis was performed to test whether the slope was significantly different from zero (P<.05), using the 2-tailed *t* test.

Results

Patients

Between January 2010 and December 2012, 21 patients met the eligibility criteria and were enrolled in the study. Of 21 patients, 4D-CT images were acquired as standard of care for all patients. FEV1, FEV_1/FVC, and SPECT data were acquired for 16, 15, and 16 patients, respectively. Data for the other patients were not available because of withdrawal from the clinical trial or incorrect data acquisition. Eighteen patients, for whom PFT and/or SPECT data was available, were included in the analysis. Characteristics of 18 patients are shown in Table 1. Several patients received repeat 4D-CT scans, and the one acquired closest to the SPECT scan time was selected for the analysis. Compared to 4D-CT, the average interval was 56 ± 53 days, and the differences in dose delivered prior to the measurement was 1 ± 3 Gy for PFT, 9 ± 10 days, and 4 ± 13 Gy for SPECT. Variable intervals and the dose differences were mainly due to logistical reasons, such as patient availability, machine availability, and patient no-show.

Figure 1 shows the relationship between FEV_1/FVC and V_{4DCT}^{HU} defect parameters for 15 patients. FEV_1/FVC decreased significantly with decreasing lowest 25th percentile V_{4DCT}^{HU}value (R=0.73, P<.01) and with increasing defect volume (R=−0.65, P<.01) and %defect volume (R=−0.63, P=.01). Table 2 shows correlations between V_{4DCT} defect parameters and PFT measurements. In general, both V_{4DCT}^{HU} and V_{4DCT}^{Jac}, demonstrated significant, moderate correlations with FEV_1 and FEV_1/FVC, indicating that severe V_{4DCT} defect is correlated with impaired global lung function. V_{4DCT}^{Jac}, had slightly stronger correlations, especially with FEV_1, than V_{4DCT}^{HU}.

4D-CT ventilation versus SPECT ventilation

Figure 2a shows a comparison between V_{4DCT}^{HU} and V_{SPECT} for patient 16, showing a good correlation and large separation between the probability density functions of V_{4DCT}^{HU} in V_{SPECT} defect regions and nondefect regions. The mean V_{4DCT}^{HU} value in V_{SPECT} nondefect regions (0.06 ± 0.06) was higher than in defect regions (0.02 ± 0.04), showing a clear separation between the peaks of the 2 probability density functions. The DSC for $V_{4DCT}^{HU}$and V_{SPECT} defect regions was 0.46. In contrast, patient 18 showed a poor correlation and small separation between the probability density functions of V_{4DCT}^{HU} in V_{SPECT} defect regions and nondefect regions (Fig. 2b). The mean V_{4DCT}^{HU} value in V_{SPECT} nondefect regions (0.11 ± 0.08) was only slightly higher than in defect regions (0.09 ± 0.08). The DSC was 0.35.
High V_{SPECT} values were noted along the border between the left lung and mediastinum due to image registration errors, resulting in erroneous defect regions along the left chest wall. Both patient 16 and 18 showed nonsevere central airway depositions in V_{SPECT}. V_{4DCT} values in V_{SPECT} defect regions and nondefect regions for 16 patients are summarized in Table 3. Both V_{4DCT}^{HU} and V_{4DCT}^{Jac} demonstrated significantly higher values in nondefect regions than in defect regions, whether or not 6 patients with severe central airway depositions in V_{SPECT} were excluded from the analysis. The average DSCs for the spatial overlap with V_{SPECT} regions were found to be only moderate (0.39 ± 0.11 for V_{4DCT}^{HU}; 0.36 ± 0.13 for V_{4DCT}^{Jac}).

Figure 3 shows ventral-to-dorsal gradients of V_{4DCT} and V_{SPECT} for 16 patients. Both V_{4DCT}^{HU} and V_{4DCT}^{Jac} demonstrated strong, but statistically nonsignificant ventral-to-dorsal gradients (V_{4DCT}^{HU} R^2=0.69, *P*=.08; V_{4DCT}^{Jac} R^2=0.68, *P*=.09), indicating higher ventilation in dorsal regions than in ventral regions. V_{SPECT} showed a strong, significant gradient (R^2=0.96, *P*<.01). For 6 patients with severe central airway depositions in V_{SPECT}, the ventral-to-dorsal gradient was still strong, but statistically nonsignificant (R^2=0.74, *P*=.06).

Discussion

This study demonstrated significant moderate correlations between V_{4DCT} defect parameters and PFT measurements (FEV_1 and FEV_1/FVC), significantly lower V_{4DCT} in VSPECT defect regions than in nondefect regions, moderate DSCs between V_{4DCT} and VSPECT defect regions, and moreover strong ventral-to-dorsal gradients. These results provide evidence toward the validation of 4D-CT ventilation imaging. PFT and SPECT ventilation imaging are widely accepted clinical standard methods for the evaluation of global and regional lung function, respectively. This is the first investigation to compare 4D-CT ventilation imaging with PFT in a cohort of thoracic cancer patients. Murphy et al (39) compared biphasic (end-expiration and end-inspiration) breath-hold CT-based ventilation with PFT measurements for 126 COPD patients and found strong correlations (0.73-0.88). There are several major differences from our study, including CT image quality, breathing maneuver and patient characteristics, which might have led to stronger correlations compared to our study. Other modalities including hyperpolarized gas MR 32, 33, 40 were found to correlate significantly with PFT. Stavngaard et al (41) reported the correlation of 0.5 (P<.05) between FEV_1 and ^{81m}Kr SPECT ventilated volume, which was similar to our study (FEV_1 vs V_{SPECT} defect volume R=−0.54, P=.04). Several investigators compared 4D-CT ventilation imaging with other modalities, including ^{99m}Tc-DTPA SPECT ventilation (20) and hyperpolarized ^{3}He MR ventilation (21) for lung cancer patients. Reasonable overlaps of defect regions were observed for MR ventilation (21). Overall only poor overlaps of percentile lung regions were reported for SPECT ventilation, whereas the overlap was relatively better in poorly ventilated regions than in well-ventilated regions (20). We found moderate DSCs between V_{4DCT} and V_{SPECT} defect regions, which were consistent with data from Castillo et al (20). Only moderate DSCs may be, at least in part, the result of spatial resolution difference. High resolution 4D-CT ventilation images provide more details and detect smaller defect regions compared to low resolution SPECT ventilation images. V_{4DCT} demonstrated significantly higher values in V_{SPECT} nondefect regions than in defect regions. However, it is unknown whether or not this is clinically significant. Proving clinical significance would ultimately require clinical trials to test a clinically relevant hypothesis.

There are several limitations in this study, including 4D-CT artifacts and limited quality of SPECT ventilation images. The current clinical standard 4D-CT technique with phase-based sorting often results in artifacts (42). In this study, we used phase-based sorting and anatomic similarity-based sorting to use the image with fewer artifacts for the analysis, though there were residual artifacts. Recently Yamamoto et al (24) demonstrated that 4D-CT artifacts are an important source of variations in 4D-CT ventilation imaging. Future developments of strategies to improve 4D-CT may increase the correlation with PFT and SPECT ventilation. Even though ^{99m}Tc-DTPA SPECT ventilation imaging is a widely accepted clinical standard method for evaluating regional lung function, it provides images of limited quality due to low resolution and

central airway depositions observed frequently in patients with COPD (7). Considering these limitations, SPECT ventilation imaging does not necessarily provide a ground truth. For future studies, comparisons with high-quality ventilation images such as xenon CT with dual-energy CT 12, 43 may provide a better understanding on the physiological significance of 4D-CT ventilation imaging.

There are several major differences between 4D-CT and PFT or SPECT, including the time, dose delivered prior to the measurement, breathing maneuver, and posture. All the measurements should ideally be acquired on the same day to minimize possible effects of time and dose differences on lung function. We consider that such effects on the results of this study would be limited for the following reasons. A subgroup analysis by dividing the patients by the median interval into 2 groups did not result in significant differences in the results between the 2 groups (data not shown). Recently Yuan et al (44) observed nonsignificant PFT changes during a course of treatment (at approximately 45 Gy) for 56 stage I-III NSCLC patients who received ≥60 Gy, whereas they observed a significant improvement in SPECT ventilation. Given that the dose difference in our patient cohort (PFT 1 ± 3 Gy; SPECT 4 ± 13 Gy) was considerably smaller than 45 Gy (44), the effect of dose difference on global and regional lung function is assumed to be minimal. Tumor growth over the interval period between the measurements (56 ± 53 days for PFT; 9 ± 10 days for SPECT) might affect lung function. A long interval between 4D-CT and PFT was due to the fact that several patients received PFT as part of the standard of care rather than specifically for the study. However, the effect is considered small because the intervals were much shorter than the tumor volume doubling time of 139 days (median) reported by Wang et al (45). SPECT provides respiration-averaged ventilation images, which may be better compared with 4D-CT ventilation images averaged over a respiratory cycle. Differences in positioning (eg, arm position, immobilization) between the 4D-CT and SPECT scans affected the quality of image registration. DIR algorithms optimized and validated to allow accurate registration to low-dose CT images of SPECT may increase the correlations. Given these limitations, the correlations between 4D-CT ventilation and PFT or SPECT ventilation found in this study would represent lower bounds to the true correlation.

Conclusions

An 18-patient study demonstrated significant correlations between 4D-CT ventilation images and PFT as well as SPECT ventilation images, providing evidence toward the validation of 4D-CT ventilation imaging. Further studies are needed to explore the physiological and clinical significance of 4D-CT ventilation imaging.

References

1. Mehta V. Radiation pneumonitis and pulmonary fibrosis in non-small cell lung cancer: Pulmonary function, prediction, and prevention. Int J Radiat Oncol Biol Phys 2005;63:5-24.

2. Marks LB, Bentzen SM, Deasy JO, et al. Radiation dose-volume effects in the lung. Int J Radiat Oncol Biol Phys 2010;76:S70- S76.

3. Palma DA, Senan S, Tsujino K, et al. Predicting radiation pneumonitis after chemoradiation therapy for lung cancer: An international individual patient data meta-analysis. Int J Radiat Oncol Biol Phys 2013; 85:444-450.

4. Abratt RP, Willcox PA, Smith JA. Lung cancer in patients with borderline lung functions - zonal lung perfusion scans at presentation and lung function after high dose irradiation. Radiother Oncol 1990; 19:317-322.

5. Seppenwoolde Y, De Jaeger K, Boersma LJ, et al. Regional differences in lung radiosensitivity after radiotherapy for non-small-cell lung cancer. Int J Radiat Oncol Biol Phys 2004;60:748-758.

6. Vinogradskiy Y, Castillo R, Castillo E, et al. Use of 4-dimensional computed tomography-based ventilation imaging to correlate lung dose and function with clinical outcomes. Int J Radiat Oncol Biol Phys 2013;86:366-371.

7. Petersson J, Sanchez-Crespo A, Larsson SA, et al. Physiological imaging of the lung: Single-photon-emission computed tomography (SPECT). J Appl Physiol 2007;102:468-476.

8. Harris RS, Schuster DP. Visualizing lung function with positron emission tomography. J Appl Physiol 2007;102:448-458.

9. Edelman RR, Hatabu H, Tadamura E, et al. Noninvasive assessment of regional ventilation in the human lung using oxygen-enhanced magnetic resonance imaging. Nat Med 1996;2:1236-1239.

10. van Beek EJ, Wild JM, Kauczor HU, et al. Functional MRI of the lung using hyperpolarized 3-helium gas. J Magn Reson Imaging 2004;20: 540-554.

11. Bauman G, Lutzen U, Ullrich M, et al. Pulmonary functional imaging: Qualitative comparison of Fourier decomposition MR imaging with SPECT/CT in porcine lung. Radiology 2011;260:551-559.

12. Chae EJ, Seo JB, Goo HW, et al. Xenon ventilation CT with a dual energy technique of dual-source CT: initial experience. Radiology 2008;248:615-624.

13. Guerrero T, Sanders K, Noyola-Martinez J, et al. Quantification of regional ventilation from treatment planning CT. Int J Radiat Oncol Biol Phys 2005;62:630-634.

14. Guerrero T, Sanders K, Castillo E, et al. Dynamic ventilation imaging from four-dimensional computed tomography. Phys Med Biol 2006; 51:777-791.

15. Reinhardt JM, Ding K, Cao K, et al. Registration-based estimates of local lung tissue expansion compared to xenon CT measures of specific ventilation. Med Image Anal 2008;12:752-763.

16. Yamamoto T, Kabus S, von Berg J, et al. Impact of four-dimensional computed tomography pulmonary ventilation imaging-based functional avoidance for lung cancer radiotherapy. Int J Radiat Oncol Biol Phys 2011;79:279-288.

17. Simpson DR, Lawson JD, Nath SK, et al. Utilization of advanced imaging technologies for target delineation in radiation oncology. J Am Coll Radiol 2009;6:876-883.

18. Fuld MK, Easley RB, Saba OI, et al. CT-measured regional specific volume change reflects regional ventilation in supine sheep. J Appl Physiol 2008;104:1177-1184.

19. Du K, Bayouth JE, Cao K, et al. Reproducibility of registration-based measures of lung tissue expansion. Med Phys 2012;39:1595-1608.

20. Castillo R, Castillo E, Martinez J, et al. Ventilation from four dimensional computed tomography: Density versus Jacobian methods. Phys Med Biol 2010;55:4661-4685.

21. Mathew L, Wheatley A, Castillo R, et al. Hyperpolarized (3)He magnetic resonance imaging: Comparison with four-dimensional x ray computed tomography imaging in lung cancer. Acad Radiol 2012; 19:1546-1553.

22. Yamamoto T, Kabus S, von Berg J, et al. Reproducibility of four dimensional computed tomography-based lung ventilation imaging. Acad Radiol 2012;19:1554-1565.

23. Johnston E, Diehn M, Murphy JD, et al. Reducing 4D CT artifacts using optimized sorting based on anatomic similarity. Med Phys 2011; 38:2424-2429.

24. Yamamoto T, Kabus S, Lorenz C, et al. 4D CT lung ventilation images are affected by the 4D CT sorting method. Med Phys 2013;40:101907.

25. Kabus S, Lorenz C. Fast elastic image registration Proc. of the Medical Image Analysis For The Clinic - A Grand Challenge. MICCAI 2010;81-89.

26. Kabus S, Klinder T, Murphy K, et al. Evaluation of 4D-CT Lung Registration. In: Yang GZ, Hawkes DJ, Rueckert D, et al., editors. London, UK: Proc of MICCAI; 2009. p. 747-754.

27. Murphy K, van Ginneken B, Reinhardt JM, et al. Evaluation of registration methods on thoracic CT: The EMPIRE10 challenge. IEEE Trans Med Imaging 2011;30:1901-1920, http://empire10.isi.uu.nl/.

28. Simon BA. Non-invasive imaging of regional lung function using x-ray computed tomography. J Clin Monit Comput 2000;16:433- 442.

29. Kipritidis J, Siva S, Hofman MS, et al. Validating and improving CT ventilation imaging by correlating with ventilation 4D-PET/CT using (68)Ga-labeled nanoparticles. Med Phys 2014;41:011910.

30. Miller MR, Hankinson J, Brusasco V, et al. Standardisation of spirometry. Eur Respir J 2005;26:319-338.

31. de Lange EE, Altes TA, Patrie JT, et al. Evaluation of asthma with hyperpolarized helium-3 MRI: Correlation with clinical severity and spirometry. Chest 2006;130:1055-1062.

32. Kirby M, Svenningsen S, Owrangi A, et al. Hyperpolarized 3He and 129Xe MR imaging in healthy volunteers and patients with chronic obstructive pulmonary disease. Radiology 2012;265:600- 610.

33. Mathew L, Gaede S, Wheatley A, et al. Detection of longitudinal lung structural and functional changes after diagnosis of radiation-induced lung injury using hyperpolarized 3He magnetic resonance imaging. Med Phys 2010;37:22-31.

34. Hudson HM, Larkin RS. Accelerated image reconstruction using ordered subsets of projection data. IEEE Trans Med Imaging 1994;13: 601-609.

35. Kauczor HU, Markstaller K, Puderbach M, et al. Volumetry of ventilated airspaces by 3He MRI: Preliminary results. Invest Radiol 2001;36:110-114.

36. Dice LR. Measures of the amount of ecologic association between species. Ecology 1945;26:297-302.

37. Petersson J, Rohdin M, Sanchez-Crespo A, et al. Posture primarily affects lung tissue distribution with minor effect on blood flow and ventilation. Respir Physiol Neurobiol 2007;156:293-303.

38. Henderson AC, Sa RC, Theilmann RJ, et al. The gravitational distribution of ventilation-perfusion ratio is more uniform in prone than supine posture in the normal human lung. J Appl Physiol 2013;115:313-324.

39. Murphy K, Pluim JP, van Rikxoort EM, et al. Toward automatic regional analysis of pulmonary function using inspiration and expiration thoracic CT. Med Phys 2012;39:1650-1662.

40. Fain SB, Gonzalez-Fernandez G, Peterson ET, et al. Evaluation of structure-function relationships in asthma using multidetector CT and hyperpolarized He-3 MRI. Acad Radiol 2008;15:753-762.

41. Stavngaard T, Sogaard LV, Mortensen J, et al. Hyperpolarized 3He MRI and 81mKr SPECT in chronic obstructive pulmonary disease. Eur J Nucl Med Mol Imaging 2005;32:448-457.

42. Yamamoto T, Langner U, Loo BW Jr, et al. Retrospective analysis of artifacts in four-dimensional CT images of 50 abdominal and thoracic radiotherapy patients. Int J Radiat Oncol Biol Phys 2008;72:1250-1258.

43. Honda N, Osada H, Watanabe W, et al. Imaging of ventilation with dual-energy CT during breath hold after single vital-capacity inspiration of stable xenon. Radiology 2012;262:262-268.

44. Yuan ST, Frey KA, Gross MD, et al. Changes in global function and regional ventilation and perfusion on SPECT during the course of radiotherapy in patients with non-small-cell lung cancer. Int J Radiat Oncol Biol Phys 2012;82:e631-e638.

45. Wang J, Mahasittiwat P, Wong KK, et al. Natural growth and disease progression of non-small cell lung cancer evaluated with 18F-fluorodeoxyglucose PET/CT. Lung Cancer 2012;78:51-56.

Table 1. Patient characteristics

Parameter	Value
Age (y)	67 ± 12
Sex	
Male	15 (83.3)
Female	3 (16.7)
FEV_1 (%pred)*	67 ± 29
FVC (%pred)†	80 ± 24
FEV1/FVC (%)‡	69 ± 24
DL_{CO} (%pred)§	79 ± 25
Histology	
Lung cancer	14 (77.8)
Thoracic paraganglioma	1 (5.6)
Metastases to the lung	3 (16.6)
Clinical stage‖	
I	3 (20.0)
II	2 (13.3)
III	6 (40.0)
IV	4 (26.7)
Lung volume (l)¶	
Peak exhalation	3.6 ± 1.7
Peak inhalation	4.2 ± 1.8

Abbreviations: DL_{co} = diffusing capacity of the lung for carbon monoxide; FEV_1 = forced expiratory volume in 1 second; FVC = forced vital capacity.
Data are means ± SD or numbers with percentages in parentheses.

∗ Available for 16 patients.
† Available for 14 patients.
‡ Available for 15 patients.
§ Available for 13 patients.
‖ For 15 patients with primary lung cancer or thoracic paraganglioma.
¶ Determined by the segmentation method for the 4D-CT images (see *Methods and Materials*).

Table 2. Correlations between 4D-CT ventilation defect parameters and pulmonary function test (PFT) measurements

PFT parameter	V_{4DCT}^{HU}			V_{4DCT}^{Jac}		
	25th Percentile	**Defect volume**	**% Defect volume**	**25th Percentile**	**Defect volume**	**% Defect volume**
FEV_1(%pred)*	0.45 (0.08)	−0.56 (0.03)	−0.43 (0.10)	0.68 (<0.01)	−0.66 (<0.01)	−0.68 (<0.01)
FEV_1/FVC (%)†	0.73 (<0.01)	−0.65 (<0.01)	−0.63 (0.01)	0.73 (<0.01)	−0.64 (0.01)	−0.64 (0.01)

Abbreviations: V_{4DCT}^{HU} = 4D-CT ventilation with Hounsfield unit (HU)-change metric, V_{4DCT}^{Jac} = 4D-CT ventilation with Jacobian metric, FEV_1 = forced expiratory volume in 1 s, FVC = forced vital capacity.

Data are Pearson correlation coefficients (R). Values in parentheses are *P* values.

∗ Available for 16 patients.

† Available for 15 patients.

Table 3. 4D-CT ventilation in SPECT defect regions versus in SPECT nondefect regions

Central airway depositions in V_{SPECT}	V_{4DCT}^{HU}			V_{4DCT}^{Jac}		
	V_{SPECT} defect	**V_{SPECT} nondefect**	***P* Value**	**V_{SPECT} defect**	**V_{SPECT} nondefect**	***P* Value**
None or nonsevere (*n*=10)	0.056 (0.041)	0.093 (0.058)	<.01	0.071 (0.046)	0.088 (0.051)	.03
Severe (*n*=6)	0.037 (0.028)	0.047 (0.027)	.05	0.023 (0.007)	0.030 (0.007)	.02
All (*n*=16)	0.049 (0.036)	0.076 (0.053)	<.01	0.053 (0.043)	0.067 (0.050)	<.01

Abbreviations:
V_{4DCT}^{HU} = 4D-CT ventilation with Hounsfield unit (HU)-change metric,
V_{4DCT}^{Jac} = 4D-CT ventilation with Jacobian metric, V_{SPECT} = SPECT ventilation.
Data are mean V_{4DCT} values in V_{SPECT} defect regions and nondefect regions. Values in parentheses are ±SD.

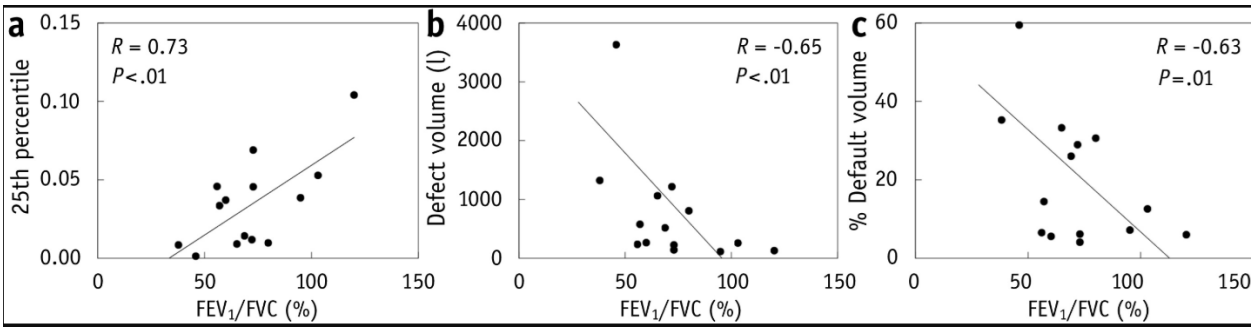

Fig. 1. FEV_1/FVC (%) versus V_{4DCT}^{HU} defect parameters: (a) 25th percentile value, (b) absolute defect volume (l), and (c) % of defect volume for 15 patients. The lines of best fit are also shown.

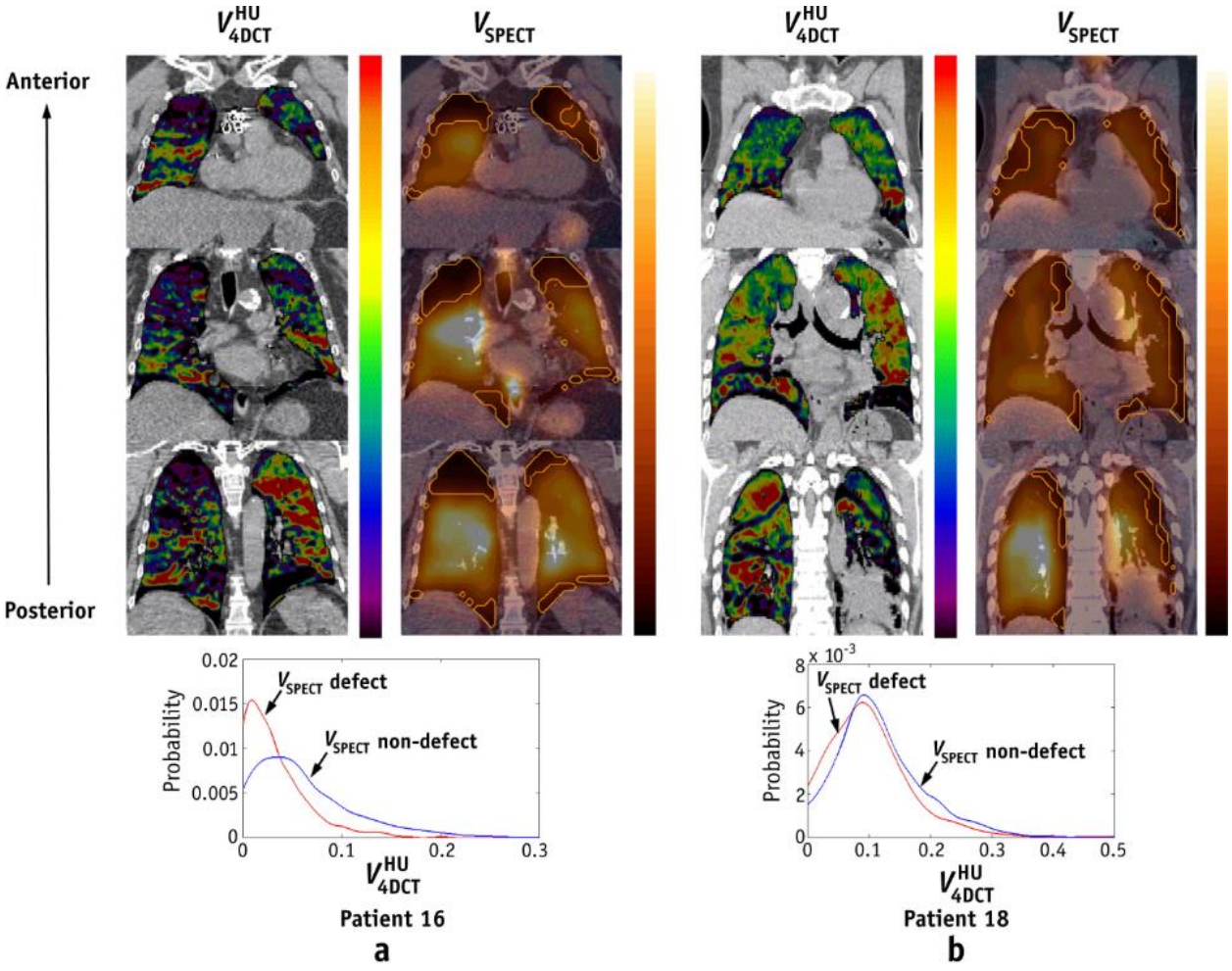

Fig. 2. Comparison of V_{4DCT}^{HU} and V_{SPECT} for (a) patient 16, showing a large separation between the probability density functions of V_{4DCT}^{HU} in V_{SPECT} defect regions and nondefect regions, and (b) patient 18, showing a small separation. Orange outlines in V_{SPECT} denote defect regions. Both V_{4DCT}^{HU} and V_{SPECT} are shown with a scale from zero to the 90th percentile value.

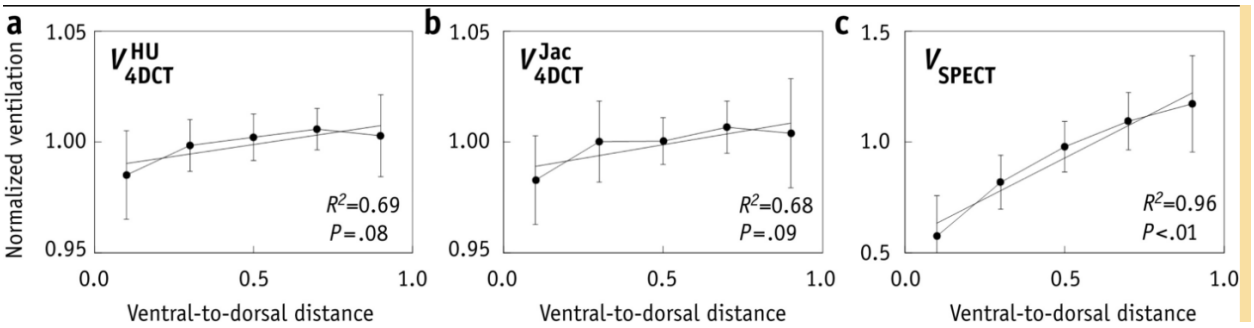

Fig. 3. Ventral-to-dorsal gradients of (a) V^{HU}_{4DCT} (y=0.02x+0.99), (b) V^{Jac}_{4DCT} (y=0.02x+0.99) and (c) V_{SPECT}(y=0.73x+0.56) for all 16 patients for whom V_{SPECT} was available. Each data point (error bar) represents the mean value (±SD) of globally normalized ventilation in a coronal section region of interest.